ORIGINAL RESEARCH   **Open Access**

CrossMark

Biokinetic and dosimetric aspects of $^{64}CuCl_2$ in human prostate cancer: possible theranostic implications

Sergio Righi[1], Martina Ugolini[1], Gianluca Bottoni[2], Matteo Puntoni[3], Massimiliano Iacozzi[2], Francesco Paparo[4], Manlio Cabria[2], Luca Ceriani[5], Monica Gambaro[1], Luca Giovanella[5] and Arnoldo Piccardo[2*]

Abstract

Background: The aim of the present study is to evaluate the kinetics and dosimetry of $^{64}CuCl_2$ in human prostate cancer (PCa) lesions.

We prospectively evaluated 50 PCa patients with biochemical relapse after surgery or external beam radiation therapy. All patients underwent $^{64}CuCl_2$-PET/CT to detect PCa recurrence/metastases. Volumes of interest were manually drawn for each $^{64}CuCl_2$ avid PCa lesion with a diameter > 1 cm on mpMRI in each patient. Time-activity curves for all lesions were obtained. The effective and biological half-life and the standard uptake values (SUVs) were calculated. Tumour/background ratio (TBR) curves as a function of time were considered. Finally, the absorbed dose per lesion was estimated.

Results: The mean effective half-life of $^{64}CuCl_2$ calculated in the lymph nodes (10.2 ± 1.7 h) was significantly higher than in local relapses (8.8 ± 1.1 h) and similar to that seen in bone metastases (9.0 ± 0.4 h). The mean $^{64}CuCl_2$ SUV_{max} calculated 1 h after tracer injection was significantly higher in the lymph nodes (6.8 ± 4.3) and bone metastases (6.8 ± 2.9) than in local relapses (4.7 ± 2.4). TBR mean curve of $^{64}CuCl_2$ revealed that the calculated TBR_{max} value was 5.0, 7.0, and 6.2 in local relapse and lymph node and bone metastases, respectively, and it was achieved about 1 h after $^{64}CuCl_2$ injection. The mean absorbed dose of the PCa lesions per administered activity was $6.00E-2 \pm 4.74E-2 mGy/MBq$. Indeed, for an administered activity of 3.7 GBq, the mean dose absorbed by the lesion would be 0.22 Gy.

Conclusions: Dosimetry showed that the dose absorbed by PCa recurrences/metastases per administrated activity was low. The dosimetric study performed does not take into account the possible therapeutic effect of the Auger electrons. Clinical trials are needed to evaluate ^{64}Cu internalization in the cell nucleus that seems related to the therapeutic effectiveness reported in preclinical studies.

Keywords: $^{64}CuCl_2$, Prostate cancer, Elderly, Kinetics and dosimetry, Theranostic

Background

Copper is an essential trace element that plays a fundamental role in a series of critical biochemical pathways. The metabolism of copper involves various transporters and copper-binding proteins; among these, the human copper transporter 1 (hCTR1) has been identified as the main mediator of copper uptake by cells [1–3]. Scientific evidence has shown that the metabolism of this element is markedly altered in neoplastic diseases [4–11]. Indeed, elevated levels of copper have been found in a wide range of tumour tissues (i.e. glioma, breast, gynaecological, gastric, bowel, lung and prostate neoplasms) [12–16]. Natural copper comprises two stable isotopes (^{63}Cu and ^{65}Cu) and 27 known radioisotopes, five of which are particularly promising for molecular imaging applications (^{60}Cu, ^{61}Cu, ^{62}Cu and ^{64}Cu) and two for in vivo targeted radiation therapy (^{64}Cu and ^{67}Cu) [7]. The versatility of ^{64}Cu, which decays via three processes,

* Correspondence: arnoldo.piccardo@galliera.it
[2]Department of Nuclear Medicine, Galliera Hospital, Mura delle Cappuccine 14, 16128 Genoa, Italy
Full list of author information is available at the end of the article

Righi et al. EJNMMI Research (2018) 8:18

Page 2 of 9

namely positron, electron capture and beta decays ($T_{1/2}$=12.7 h; $E_{mean\ \beta+}$ = 0.28 MeV (17.86%); $E_{mean\ \beta-}$ = 0.19 MeV (39.0%); EC (43.075%) [17], makes it the most widely studied radioisotope, in the areas of both PET imaging and the targeted radiotherapy of cancer. [18]. The beta particle emission implies a high local radiation dose that is theoretically suitable for targeted radionuclide therapy. Furthermore, the electron capture decay is followed by the emission of Auger electrons characterized by high linear energy transfer (LET); this is able to considerably increase the cytotoxic power of ^{64}Cu, if the radioisotope is targeted near or within the cell nucleus. Because of these properties, ^{64}Cu is described as the archetypal "theranostic" radioisotope, as it is potentially useful in PET/CT imaging and in radionuclide therapy [19]. A growing body of evidence suggests that ^{64}Cu may provide relevant therapeutic effects. Indeed, some preclinical in vitro and animal studies have been recently conducted on this topic [20–28]. On the other hand, little can be said about the effect of ^{64}CuCl$_2$ in humans, and only two preliminary reports have confirmed the therapeutic effect of ^{64}CuCl$_2$ in patients affected by relapsing malignancies (i.e. glioblastoma, prostate and uterine cancer) [29, 30]. However, two pioneering studies, on the diagnostic role of ^{64}CuCl$_2$-PET/CT in human prostate cancer, reported that this imaging procedure has high sensitivity in detecting prostate cancer relapse [4, 8]. In this field, the International Atomic Energy Agency (IAEA) has implemented a coordinated research project entitled "Copper-64 Radiopharmaceuticals for Theranostic Applications", which is focused on the application of theranostic properties of ^{64}Cu and on developing and evaluating the most promising ^{64}Cu-chelated targeting agents for the therapy and diagnosis of human diseases (http://cra.iaea.org/cra/stories/2015-12-22-F22067-Copper-64-Radiopharmaceuticals.html).

In a recent prospective paper, we investigated the ability of ^{64}CuCl$_2$-PET/CT as a diagnostic agent to detect prostate cancer (PCa) recurrence in 50 patients with biochemical relapse, after prostatectomy or external beam radiation therapy (EBRT) [4]. In the same group of patients, we also compared the ^{64}CuCl$_2$-PET/CT results with those of ^{18}F-Choline PET/CT and multiparametric magnetic resonance imaging (mpMRI). In parallel, we evaluated the biodistribution of ^{64}CuCl$_2$ and the absorbed dose to organs in all patients. The biodistribution of ^{64}CuCl$_2$ and the absorbed dose to organs were evaluated by considering as the source organs those with the highest uptake of ^{64}CuCl$_2$ (namely liver, kidneys, pancreas, gallbladder wall, salivary glands and spleen). The effective dose was also calculated by using the coefficients of radiosensitivity of the organs present in publications 60 and 103 of the International Commission on Radiological Protection (ICRP) [31, 32].

In the present study, by using the same source data, we evaluated (i) the kinetic aspects, (ii) the tumour/background ratio (TBR) as a function of time and (iii) the absorbed dose of ^{64}Cu dichloride in PCa lesions.

In addition, we extended the previous evaluation [4] of the dose absorbed by the organs and the effective dose by including the analysis of the red marrow as a source organ.

Methods
The local ethics committee and the "Agenzia Italiana del Farmaco", a public agency of the Italian Ministry of Health, approved this study. All subjects provided written informed consent. The trial was registered in the European Clinical Trial Database (EudraCT number 2014-005140-18).

Patient population and diagnostic protocol
The population analyzed was the same as in the previous study [4]. Fifty PCa patients were prospectively evaluated and all underwent ^{64}CuCl$_2$-PET/CT and mpMRI within 15 days of one another. ^{64}CuCl$_2$-PET/CT were acquired 1, 4 and 24 h after tracer injection [4]. The analysis presented in this paper concerns PCa lesions with a diameter larger than 1 cm (0.52 mL) detected by ^{64}CuCl$_2$-PET/CT; thus, 59 lesions in 35 patients were considered: 29 local recurrences, 21 lymph node metastases and 9 bone metastases. The volume mean values of the three sites of disease were 19.5 ± 25.9 mL, 4.7 ± 5.2 mL and 7.1 ± 9.7 mL, respectively.

Lesion contouring
To evaluate kinetics and tumour dosimetry, volumes of interest (VOIs) were manually drawn by an experienced nuclear medicine physician and by one experienced radiologist on the ^{64}CuCl$_2$-PET/CT images acquired 1 h after tracer injection. Specifically, the VOIs were drawn after co-registration (i.e. multimodal fusion imaging) between mpMRI and PET/CT images, which was performed, only in the case of positive mpMRI findings with diameter > 1 cm, by means of dedicated software developed for research purposes (Quanta Oncology, Camelot Biomedical Systems, Genoa, Italy) [33, 34]. These VOIs were then transferred to the other two PET/CT datasets (at 4 and 24 h) of each patient, after proper co-registration with mpMRI images. Furthermore, in order to evaluate the muscle radioactivity concentration as a function of time, a spherical VOI was drawn on each PET/CT image of the upper thigh of each patient.

Lesion kinetics
The mean concentration of ^{64}CuCl$_2$ radioactivity in the VOIs was recorded for all PET datasets. Time-activity curves (as a percentage of injected activity/mL) for all

Righi *et al. EJNMMI Research* (2018) 8:18

Page 3 of 9

lesions were fitted as bi-exponential functions [35]. The effective half-life was evaluated by fitting the radioactivity concentration values of the late PET images (i.e. 4 and 24 h after injection) with a mono-exponential curve. Standard uptake values (SUVs, i.e. SUV_{mean} and SUV_{max}) in all VOIs were also recorded, and their values were recalculated from their respective kinetic curves at the reference time of 1 h after administration. Furthermore, the mean concentration values for tumours, the main organs at risk (namely liver, kidneys and pancreas) and the muscle were calculated from the corresponding kinetic curves at 1, 4 and 24 h after administration. To conduct the analysis of the organs at risk, the kinetic curves obtained in the previous study were used [4].

In order to take into account the partial volume effect (PVE), in our study, the recovery correction method was used [36–39]. This method is based on numerical coefficients (recovery coefficients, RCs) that are experimentally measured by using radioactive phantoms. RCs are used to recover the radioactivity concentration measured by the PET tomograph and are obtained as the ratio between the PET-measured radioactivity concentration and the actual radioactivity concentration within the hot spheres simulating PCa lesions. To this end, the six spheres of various diameters (10, 13, 17, 22, 28 and 37 mm), which are part of the NEMA IEC Body Phantom insert (http://www.spect.com/pub/NEMA_IEC_Body_Phantom_Set.pdf), were filled with a known concentration of $^{64}CuCl_2$. To simulate the background, the body phantom chamber was also filled with radioactivity. Three different phantom TBR (3, 9 and 20) were chosen in order to reproduce the clinical range patients' tumour/background ratio (namely about 2–15). The PET/CT acquisition of the phantom was performed by using the same clinical protocol setup described in the previous study [4]. Six spherical VOIs, having the same diameters of the spheres of NEMA phantom, were drawn on the corresponding spheres on PET/CT images. In order to calculate RC values, the mean radioactivity concentration was measured in each VOI by means of PMOD software (PMOD, Zurich, Switzerland). The RC curves (Additional file 1: Figure S1) were obtained by fitting RC experimental data with the function:

$$RC = \alpha \cdot \left(\frac{V}{V + \beta} \right)^{\gamma} \tag{1}$$

where V is the volume of the sphere (α, β and γ are the fit parameters).

Statistical analysis
Continuous and categorical factors were described by using mean, standard deviation (SD), quartiles, minimum, maximum and absolute/relative (%) frequencies, respectively. Box plots were adopted to visually describe

data, and differences among groups were tested by using non-parametric tools (Kruskal-Wallis equality-of-populations rank test and Mann-Whitney test). No multiple testing adjustments were applied. All p values (two-sided) < 0.05 were considered statistically significant. The statistical software adopted was STATA v.14.2 (College Station, TX, USA).

Tumour/background ratio
The TBR of all lesions was evaluated. The background radioactivity concentration was obtained by calculating the mean value of four VOIs drawn at 1 cm from each lesion. Furthermore, to evaluate the TBR_{max} and TBR_{mean} of $^{64}CuCl_2$-PET/CT, the three values of TBR were fitted with a bi-exponential curve as a function of time. The mean TBR curve was obtained by averaging the TBR fitting curves of all tumours in each site of disease.

Tumours and red marrow dosimetry
To perform the dosimetry of the PCa lesions, the accumulated activity (the sum of all nuclear transitions that occur inside the tumour) for all lesions was calculated as the area under the time-activity curve, and the time-integrated activity coefficient (τ) was obtained dividing the accumulated activity by the administered activity. The activity considered in the tumours was corrected for the PVE. The absorbed dose per administrated activity for each lesion was calculated by using the Medical Internal Radiation Dose (MIRD) system [40, 41]. Using OLINDA/EXM software [42], S-factors for spheres for ^{64}Cu (in mGy/MBq*h) were obtained by fitting tumour masses (m, in grams), in the range of our study, with the function (Additional file 2: Figure S2):

$$S = \frac{A}{m^B} \tag{2}$$

where A and B are the fit parameters.

For local and lymph node lesions, a density of 1 g/mL was considered, while for bone tumours, a mean density of 1.2 g/mL was estimated from CT Hounsfield numbers.

To calculate the dose absorbed by the red marrow, VOIs corresponding to L4 and L5 were drawn in each $^{64}CuCl_2$-PET/CT dataset for every patient (50 in total) [43]. Indeed, the red marrow in these two vertebrae accounts for 6.8% of that of the entire skeleton [44]. Thus, the number of disintegrations in this vertebral region was divided by 0.068 to obtain the number of disintegrations in the entire red marrow.

Results

Lesion kinetics

PVE-corrected time-activity curves of $^{64}CuCl_2$ for the three types of lesion (local relapses and lymph node and bone metastases) showed that the uptake was rapid, reaching the maximum value approximately 1 h after $^{64}CuCl_2$ administration (Fig. 1). The bi-exponential fitting curves highlighted a rapid clearance in the first few hours after the maximum uptake, followed by a slower tracer elimination starting from the fourth hour. The trend of $^{64}CuCl_2$ uptake over time is illustrated in Fig. 2. Table 1 summarizes the differences in mean effective (and biological) half-life, the PVE-corrected SUV_{mean} and SUV_{max} mean values 1 h after $^{64}CuCl_2$ injection, the time-integrated activity coefficients and the absorbed dose (per administrated activity), among the three sites of PCa relapse. A box plot representation of these parameters is shown in Fig. 3. A statistically significant difference in terms of effective half-life was observed between local recurrences and lymph node metastases. We also found a significant difference in terms of PVE-corrected SUV_{mean} and SUV_{max} evaluated 1 h after tracer injection between local and lymph node metastases and between local recurrences and bone metastases. Furthermore, a statistically significant difference in terms of absorbed dose was observed between local relapses and lymph node metastases (Table 1). In Fig. 4, the $^{64}CuCl_2$ concentration (as a percentage of injected activity) in the PCa lesions, for each site of diseases, and in several organs is shown. Over time, the tumour concentration was about 4.5 and 2.0 times lower than in the liver and kidneys, respectively.

Tumour/background ratio

Background time-activity curves of $^{64}CuCl_2$ showed the same bi-exponential trend as the tumour time-activity curves. The maximum uptake was observed about 1 h after $^{64}CuCl_2$ administration. The typical time-activity curves of PCa relapse and background are illustrated in
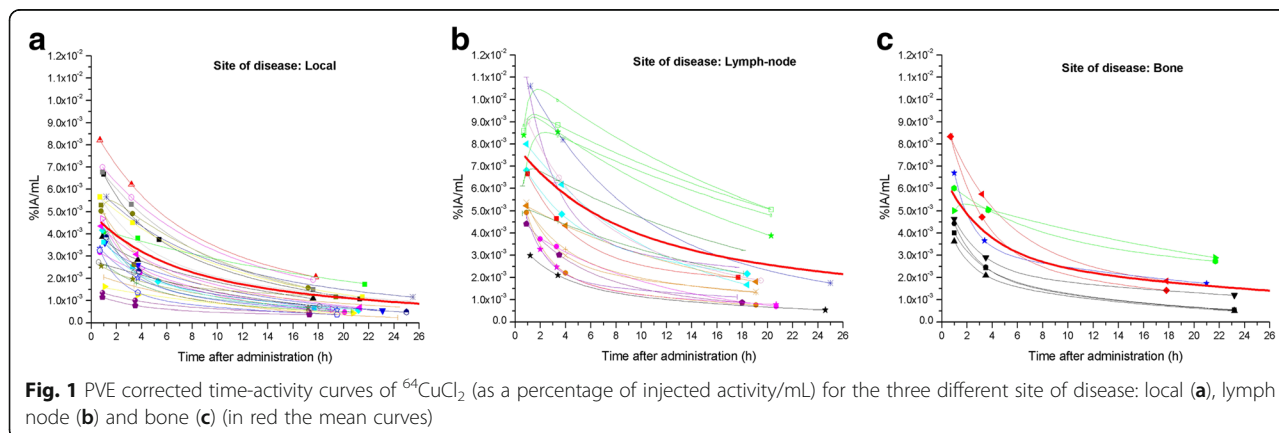
Additional file 3: Figure S3. The $^{64}CuCl_2$-PET TBR curves of the local recurrences and lymph node and bone metastases are illustrated in Fig. 5. These curves revealed that the mean TBR value (TBR_{mean}) was 5.0, 7.0 and 6.2 over 24 h, and the TBR_{max} was 6.1, 7.6 and 7.4 for local relapses and lymph node and bone metastases, respectively. The TBR_{max} was achieved about 1 h after radiopharmaceutical administration for each site of disease.
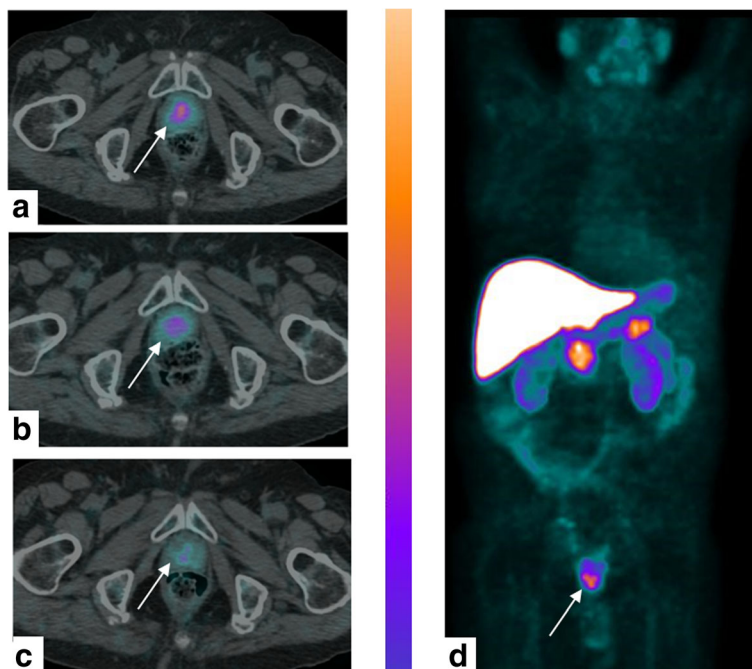
Tumours and red marrow dosimetry

The mean dose absorbed by PCa lesions per administered activity was 6.00E-2 ± 4.74E-2mGy/MBq (3.71E-2 ± 1.87E-2 mGy/MBq, 9.65E-2 ± 5.95E-2 mGy/MBq and 5.40E-2± 3.86E-2mGy/MBq for local relapses and lymph node and bone metastases, respectively. The maximum uptake by red marrow was about 2% of the injected activity, and the mean absorbed dose per administered activity was 2.26E-2 ± 9.04E-3 mGy/MBq. Thus, the effective dose was 3.10E-2 ± 8.07E-3 mSv/MBq and 2.91E-2 ± 7.83E-3 mSv/MBq when it was recalculated by using the radio-sensitivity coefficients of the organs of the ICRP protocols 60 and 103, respectively [31, 32]. The recalculated doses absorbed by the organs are reported in Table 2. In Fig. 6, the mean absorbed dose by each site of diseases and by several organs is shown. Radiation dosimetry analysis showed that the mean absorbed dose per administered activity was 4.5 and 2.3 times higher in the liver and kidneys, respectively, than in PCa lesions.

Discussion

In our study, a thorough evaluation of ^{64}Cu dichloride behaviour in human PCa was performed. Specifically, we analysed the kinetics and dosimetry of the three typical sites of PCa relapse: local recurrences, lymph node metastases and bone metastases. The kinetic analysis of the PCa lesions showed a rapid uptake within the first hour after administration, followed by a washout phase

Fig. 1 PVE corrected time-activity curves of $^{64}CuCl_2$ (as a percentage of injected activity/mL) for the three different site of disease: local (**a**), lymph node (**b**) and bone (**c**) (in red the mean curves)

Fig. 2 An 85-year-old man affected by Gleason 4+3 PCa treated with EBRT, with rising PSA level (6.0 ng/mL) and PSA doubling time of 15 months. $^{64}CuCl_2$-PET/CT images (axial and MIP) revealed focal and pathologic tracer uptake (arrows) in correspondence to the prostate apex close to the midline 1 h after the injection (**a**). An important reduction of tracer uptake was observed 4 (**b**) and 24 h (**c**) after the injection. Maximum intensity projection (**d**) visualized the differences in terms of uptake between the organsand prostate relapse

characterized by two different biological times: rapid clearance in the first hour after the maximum uptake and a slower kinetic starting from the fourth hour after the tracer injection. This behaviour was also found in the muscles and in the tissues around the tumours (i.e. background) and had already been observed in the organs in our previous study [4]. On the one hand, the time to maximum uptake was similar in both healthy and pathologic tissues. On the other hand, the effective half-life was different in each healthy tissue and in each different site of disease relapse. Indeed, the $^{64}CuCl_2$ half-life in lymph node metastases was significantly longer than in local recurrences. When the uptake intensity of $^{64}CuCl_2$ was considered, lymph node metastases and bone metastases showed significantly higher SUV_{mean} and SUV_{max} mean values than local recurrences. Our study highlighted that the mean concentration of $^{64}CuCl_2$ in PCa lesions over time was about 4.5 and 2.0 times lower than in the liver and kidneys, respectively. This result is consistent with the values already published in mice with regard to melanoma, prostate cancer and hepatocellular carcinoma [9–11]. Therefore, it can be hypothesized that this behaviour is independent of the tumour subtype.

The high $^{64}CuCl_2$ TBR in PCa recurrences/metastases, as confirmed in this study, is the most important characteristic of this tracer. Indeed, the high contrast between the lesions and the surrounding healthy tissue may considerably improve the diagnostic performance of PET/CT. On evaluating the TBR curves, we found that the $^{64}CuCl_2$ TBR_{max} was reached approximately 1 h after tracer injection.

Table 1 Summary table of the main tumour results

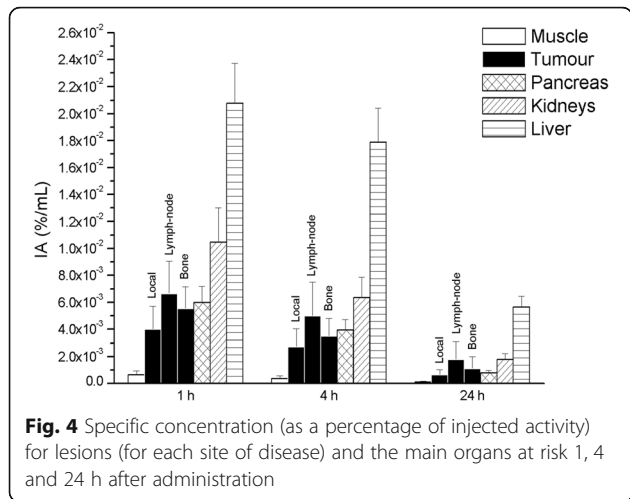|	Local recurrences	Lymph node metastasis	Bone metastasis	*p* Local vs lymph node	*p* Local vs bone	*p* Lymph node vs Bone
$T_{1/2eff}$ ($T_{1/2biol}$) (h)	8.8 ± 1.1 (28.7 ± 3.6)	10.2 ± 1.7 (51.8 ± 8.6)	9.0 ± 0.4 (30.9 ± 1.4)	**0.003**	0.9	0.4
SUV_{mean} at 1 h	3.1 ± 1.1	5.2 ± 2.1	4.3 ± 0.9	**< 0.001**	**0.003**	0.8
SUV_{max} at 1 h	4.7 ± 2.4	6.8 ± 4.3	6.8 ± 2.9	**0.02**	**0.03**	0.5
τ (h)	1.1E-2 ± 2.4E-2	6.1E-3 ± 7.8E-3	6.4E-3 ± 1.0E-2	0.3	0.2	0.8
D/A (mGy/MBq)	3.71E-2 ± 1.87E-2	9.65E-2 ± 5.95E-2	5.40E-2 ± 3.86E-2	**< 0.001**	0.1	0.6

Values are reported as mean ± standard deviation. Statistically significant differences (*p* < 0.05) are in bold

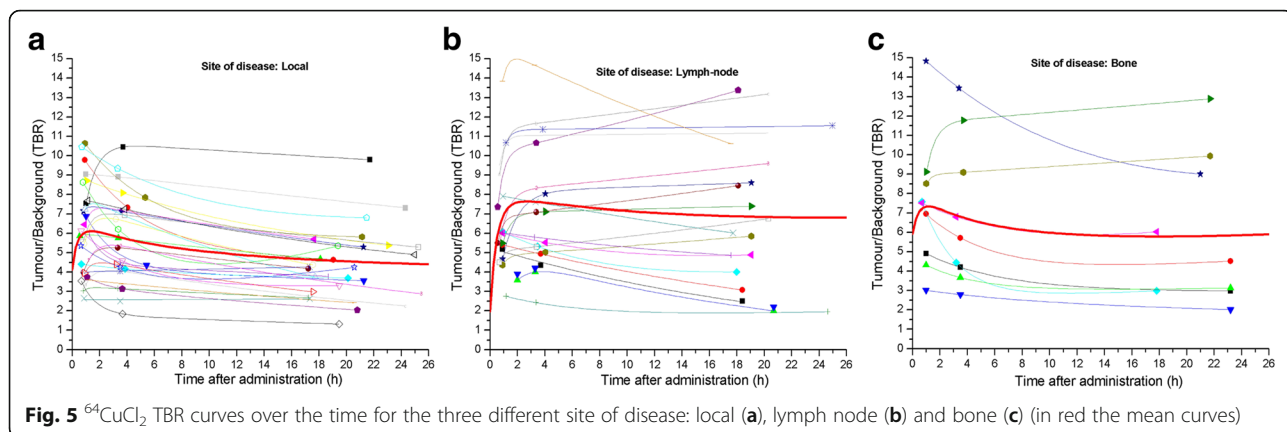Righi *et al. EJNMMI Research* (2018) 8:18

Page 6 of 9
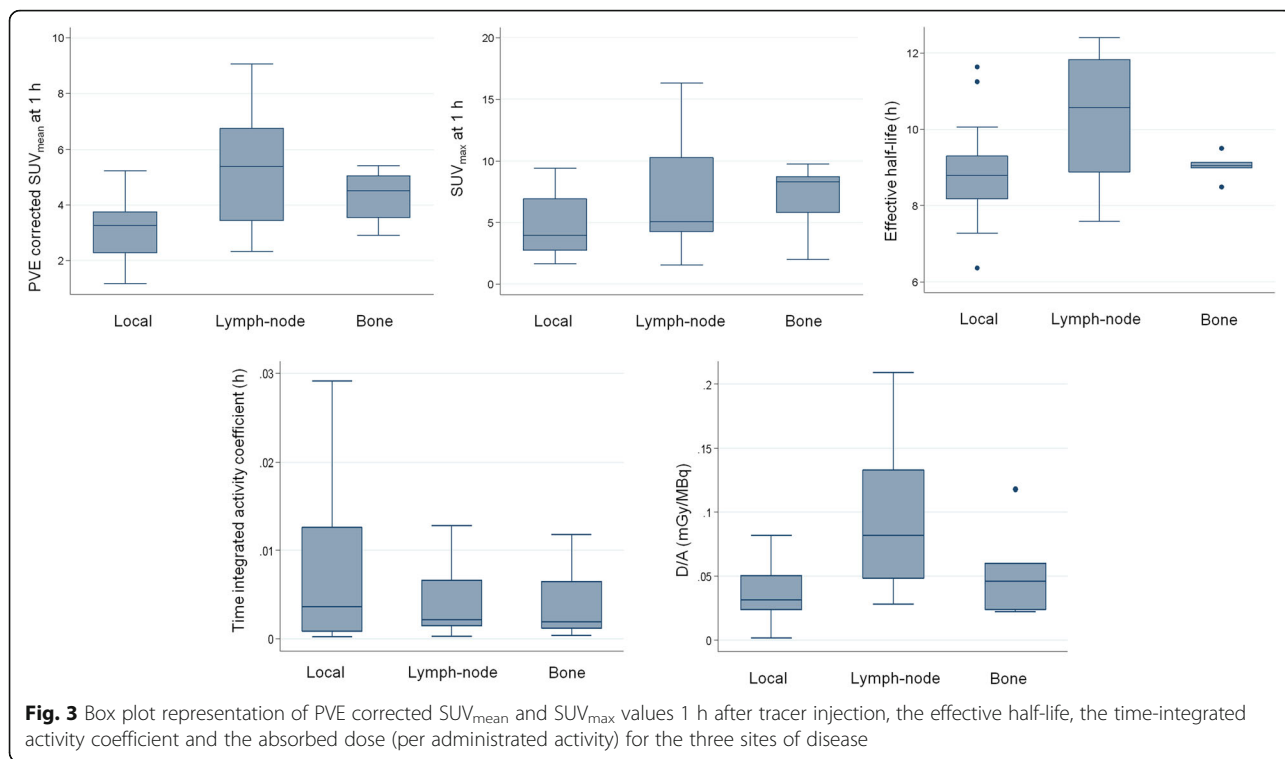
Fig. 3 Box plot representation of PVE corrected SUV_{mean} and SUV_{max} values 1 h after tracer injection, the effective half-life, the time-integrated activity coefficient and the absorbed dose (per administrated activity) for the three sites of disease

To our knowledge, this is the first study to investigate the $^{64}CuCl_2$ dosimetry of human PCa. The mean dose absorbed by the tumors per administered activity, calculated by means of the MIRD, was 6.00E-2 mGy/MBq. This absorbed dose was 4.5 and 2.3 times lower than the mean values in the liver and kidneys, respectively. For an administered activity of 3.7 GBq, the mean dose absorbed by the lesions would be 0.22 Gy. This low value seems to suggest the hypothesis that the reported therapeutic effect of $^{64}CuCl_2$ [20–30] is mainly dependent on Auger electron emission rather than on the energy released by the beta radiation. In this setting,

Fig. 4 Specific concentration (as a percentage of injected activity) for lesions (for each site of disease) and the main organs at risk 1, 4 and 24 h after administration

to be effective, ^{64}Cu should be internalized in the cell nucleus [45–47], since Auger cascade electrons have an energy spectrum dominated by a large number of very low energy electrons with a very narrow range in biological matter. Indeed, cellular and organ studies have demonstrated that when Auger emitters are introduced into the cytoplasm of cells, the effects are typical of those caused by radiation of low LET, such as photons and beta radiations [48]. On the other hand, when Auger emitters are incorporated into the cell nucleus, the LET of these electrons can cause similar biological damage to that elicited by heavier particles with high LET, such as alpha particles [49]. Therefore, the cytocidal effect of the Auger electrons of ^{64}Cu appears to be much more severe than that of beta emission; indeed, some studies report effects up to 5–25 times [50–61]. In addition, since the liver has been identified as the organ receiving the higher dose, owing to its high uptake [4, 62, 63], it is important to understand whether ^{64}Cu is internalized in the nucleus of hepatic cells or not. If it is not, the potential hepatic radiotoxicity might be induced by the beta emission component only by means of very high injected activity [4]. More detailed radiobiological studies are required to characterize the radiotoxicity and therapeutic effects of $^{64}CuCl_2$. However, to really understand whether or not the liver is the critical organ in the case of therapeutic application of $^{64}CuCl_2$, phase I clinical trials, not available at the moment, should be conducted.

Righi *et al. EJNMMI Research* (2018) 8:18

Page 7 of 9

Fig. 5 $^{64}CuCl_2$ TBR curves over the time for the three different site of disease: local (**a**), lymph node (**b**) and bone (**c**) (in red the mean curves)

Since the red marrow is a dose-limiting organ in radio-nuclide therapy, we extended the dosimetry performed in the previous study [4] and included the red marrow as a source organ, too. We found that the absorbed dose in the red marrow was 2.26E-2 mGy/MBq, i.e. 75% higher than that of previously published [4]. As expected, the absorbed doses in other organs were substantially unvaried.

Despite our encouraging results, at least few limitations should be taken into account. The lack of dynamic

Table 2 Absorbed organs dose per administered activity (± SD) for $^{64}CuCl_2$

Organ	Absorbed organ dose per administered activity (mGy/MBq)
Adrenals	2.54E-2 (± 6.60E-3)
Brain	1.04E-2 (± 3.95E-3)
Breasts	1.22E-2 (± 4.07E-3)
Gallbladder wall	7.82E-2 (± 2.99E-2)
Lower larger intestine wall	1.25E-2 (± 4.76E-3)
Upper large intestine wall	1.78E-2 (± 5.31E-3)
Small intestine	1.62E-2 (± 5.42E-3)
Stomach wall	1.70E-2 (± 5.48E-3)
Heart wall	1.80E-2 (± 5.30E-3)
Kidneys	1.39E-1 (± 3.72E-2)
Liver	2.71E-1 (± 3.37E-2)
Lungs	1.64E-2 (± 4.88E-3)
Muscle	1.34E-2 (± 4.51E-3)
Pancreas	8.39E-2 (± 4.03E-2)
Red marrow	2.26E-2 (± 9.04E-3)
Osteogenic cells	3.00E-2 (± 1.16E-2)
Skin	1.09E-2 (± 3.84E-3)
Spleen	3.63E-2 (± 1.37E-2)
Testes	1.10E-2 (± 4.14E-3)
Thymus	1.31E-2 (± 4.53E-3)
Thyroid	1.16E-2 (± 4.31E-3)
Urinary bladder wall	1.27E-2 (± 4.69E-3)
Salivary glands	3.70E-2 (± 3.70E-2)
Total body	2.09E-2 (± 5.61E-3)
Effective dose ICRP 60 (mSv/MBq)	3.10E-2 (± 8.07E-3)
Effective dose ICRP 103 (mSv/MBq)	2.91E-2 (± 7.83E-3)

Righi *et al. EJNMMI Research* (2018) 8:18

Page 8 of 9
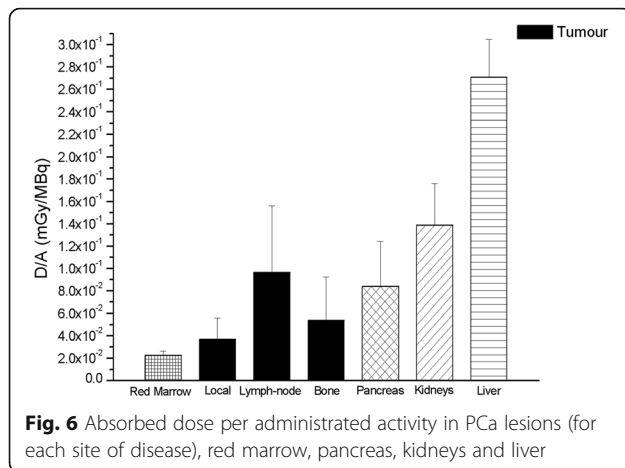
Fig. 6 Absorbed dose per administrated activity in PCa lesions (for each site of disease), red marrow, pancreas, kidneys and liver

acquisition in the uptake phase implies poor knowledge of the radionuclide behaviour immediately after administration. Furthermore, the acquisition of other time points would let better time-integrated activity coefficient and dosimetry evaluations. Finally, the absorbed dose by the red marrow was not calculated using blood sampling. However, to facilitate patient compliance, we decided not to insist on these long diagnostic procedures.

Conclusions

The high diagnostic sensitivity of $^{64}CuCl_2$ PET/CT is related to its high TBR_{max}, such a value was reached about 1 h after administration. Dosimetry based on MIRD showed that the dose absorbed by PCa recurrences/metastases per administrated activity was low and unlikely able to reach therapeutic effects. Clinical trials are needed in order to evaluate ^{64}Cu internalization in the cell nucleus that seems related to the therapeutic effectiveness reported in preclinical studies.

Additional files

Additional file 1: Figure S1. Experimental RC values for three TBR values. (TIFF 405 kb)

Additional file 2: Figure S2. S-factors specific for variable mass spheres for ^{64}Cu (OLINDA/EXM software). (TIFF 381 kb)

Additional file 3: Figure S3. Typical time-activity curve for tumour and background. (TIFF 397 kb)

Abbreviations

EBRT: External-beam radiation therapy; hCTR1: Human copper transporter 1; IAEA: International Atomic Energy Agency; ICRP: International Commission on Radiological Protection; LET: Linear energy transfer; MIRD: Medical Internal Radiation Dose; mpMRI: Multiparametric magnetic resonance imaging; PCa: Prostate cancer; PVE: Partial volume effect; RC: Recovery coefficient; SD: Standard deviation; SUV: Standard uptake value; TBR: Tumor/background ratio; VOI: Volume of interest

Authors' contributions
SR, MU and AP are the principal investigators of this research and guarantors of integrity of the entire study design and manuscript writing. MC, MG, LG and LC contributed to the study design and manuscript editing and review. GB, FP and MU analyzed the images and performed the dosimetric calculations. MP performed the statistical analysis. MI designed the acquisition of PET/CT scans and analyzed the images. All authors read and approved the final manuscript.

Ethics approval and consent to participate
This protocol was approved by the Bioethical Committee of "Regione Liguria". All procedures performed in studies involving human participants were in accordance with the ethical standards of the institutional and/or national research committee and with the 1964 Helsinki Declaration and its later amendments or comparable ethical standards. Informed consent was obtained from all individual participants included in the study.

Consent for publication
Not applicable

Competing interests
The authors declare that they have no competing interest.

Publisher's Note
Springer Nature remains neutral with regard to jurisdictional claims in published maps and institutional affiliations.

Author details
[1]Medical Physics Department, E.O. Galliera Hospital, Genoa, Italy. [2]Department of Nuclear Medicine, Galliera Hospital, Mura delle Cappuccine 14, 16128 Genoa, Italy. [3]Clinical Trial Unit, Office of the Scientific Director, Galliera Hospital, Genoa, Italy. [4]Department of Radiology, E.O. Galliera Hospital, Genoa, Italy. [5]Department of Nuclear Medicine, Oncology Institute of Southern Switzerland, Bellinzona, Switzerland.

References
1. Turski ML, Thiele DJ. New roles for copper metabolism in cell proliferation, signaling, and disease. J Biol Chem. 2009;284:717–21.
2. Huawei C, Jiu-sheng W, Otto M, et al. Reduced 64Cu uptake and tumor growth inhibition by knockdown of human copper transporter 1 in xenograft mouse model of prostate cancer. J Nucl Med. 2014;55:622–8.
3. Kim KI, Jang SJ, Park JH, et al. Detection of increased 64Cu uptake by human copper transporter 1 gene overexpression using PET with 64CuCl2 in human breast cancer xenograft model. J Nucl Med. 2014;55(10):1692–8.
4. Piccardo A, Paparo F, Puntoni M, et al. 64CuCl2 PET/CT in prostate cancer relapse. J Nucl Med. 2017;8. https://doi.org/10.2967/jnumed.117.195628.
5. Gupte A, Mumper RJ. Elevated copper and oxidative stress in cancer cells as a target for cancer treatment. Cancer Treat Rev. 2009;35:32–46.
6. Jørgensen JT, Persson M, Madsen J, et al. High tumor uptake of (64)Cu: implications for molecular imaging of tumor characteristics with copper-based PET tracers. Nucl Med Biol. 2013;40:345–50.
7. Szymański P, Frączek T, Markowicz M, et al. Development of copper based drugs, radiopharmaceuticals and medical materials. Biometals. 2012;25: 1089–112.
8. Capasso E, Durzu S, Piras S, et al. Role of (64)CuCl2 PET/CT in staging of prostate cancer. Ann Nucl Med. 2015;29:482–8.
9. Jiang L, Tu Y, Hu X, et al. Pilot study of 64Cu(I) for PET imaging of melanoma. Sci Rep. 2017;7(1):2574.
10. Peng F, Lu X, Janisse J, et al. PET of human prostate cancer xenografts in mice with increased uptake of 64CuCl2. J Nucl Med. 2006;47:1649–52.

Righi *et al. EJNMMI Research* (2018) 8:18

Page 9 of 9

11. Haiyuan Z, Huawei C, Xin L, et al. Positron emission tomography of human hepatocellular carcinoma xenografts in mice using copper (II)-64 chloride as a tracer. Acad Radiol. 2011;18:1561–8.

12. Kuo KW, Chen SF, Wu CC, et al. Serum and tissue trace elements in patients with breast cancer in Taiwan. Biol Trace Elem Res. 2002;89(1):1–11.

13. Chan A, Wong F, Arumanayagam M. "Serum ultrafiltrable copper, total copper and ceruloplasmin concentrations in gynecological carcinoma". Ann Clin Biochem. 1993;30:545–9.

14. Scanni A, Licciardello L, Trovato M, et al. Serum copper and ceruloplasmin levels in patients with neoplasias localized in the stomach, large intestine or lung. Tumori. 1977;63(2):175–80.

15. Safi R, Nelson ER, Chitneni SK, et al. Copper signaling axis as a target for prostate cancer therapeutics. Cancer Res. 2014;74(20):5819–31.

16. Panichelli P, Villano C, Cistaro A, et al. Imaging of brain tumors with copper-64 chloride: early experience and results. Cancer Biother Radiopharm. 2016;31:159–67.

17. Eckerman K, Endo A. ICRP Publication 107. Nuclear decay data for dosimetric calculations. Ann ICRP. 2008;38(3):7–96.

18. Blower PJ, Lewis JS, Zweit J. Copper radionuclides and radiopharmaceuticals in nuclear medicine. Nucl Med Biol. 1996;23:957–80.

19. Jalilain AR, Osso J. The current status and future of theranostic copper-64 radiopharmaceuticals. Iran J Nucl Med. 2017;25:1–10.

20. McMillan DD, Maeda J, Bell JJ, et al. Validation of 64Cu-ATSM damaging DNA via high-LET auger electron emission. J Radiat Res. 2015;56:784–91.

21. Connett JM, Anderson CJ, Guo LW, et al. Radioimmunotherapy with a 64Cu-labeled monoclonal antibody: a comparison with 67Cu. Proc Natl Acad Sci U S A. 1996;25(93):6814–8.

22. Qin C, Liu H, Chen K, et al. Theranostics of malignant melanoma with 64CuCl2. J Nucl Med. 2014;55:812–7.

23. Ferrari C, Asabella AN, Villano C, et al. Copper-64 dichloride as theranostic agent for glioblastoma multiforme: a preclinical study. Biomed Res Int. 2015; 2015:129764.

24. Catalogna G, Talarico C, Dattilo V, et al. The SGK1 kinase inhibitor SI113 sensitizes theranostic effects of the 64CuCl2 in human glioblastoma multiforme cells. Cell Physiol Biochem. 2017;43(1):108–19.

25. Lewis JS, Lewis MR, Cutler PD, et al. Radiotherapy and dosimetry of 64Cu-TETA-Tyr3-octreotate in a somatostatin receptor-positive, tumor-bearing rat model. Clin Cancer Res. 1999;5(11):3608–16.

26. Lewis JS, Laforest R, Buettner TL, et al. Copper-64-diacetyl-bis(N4-methylthiosemicarbazone): an agent for radiotherapy. PNAS. 2001;98(3): 1206–11.

27. Yoshii Y, Matsumoto H, Yoshimoto M, et al. Multiple administrations of 64Cu-ATSM as a novel therapeutic option for glioblastoma: a translational study using mice with xenografts. Transl Oncol. 2017;11(1):24–30.

28. Obata A, Kasamatsu S, Lewis JS, et al. Basic characterization of 64Cu-ATSM as a radiotherapy agent. Nucl Med Biol. 2005;32(1):21–8.

29. Capasso E, Valentini MC, Mirzaei S, et al. Radionuclide treatment with 64Cu-Cl2 in patients with progressive malignant gliomas. Eur J Nucl Med Mol Imaging. 2015;42(Suppl 1):S12.

30. Valentini G, Panichelli P, Villano C, et al. 64CuCl2: new theranostic agent. Nucl Med Biol. 2014;41(7):638.

31. 1990 Recommendations of the International Commission on Radiological Protection. Ann. ICRP 1991 21 (1–3)1–201.

32. The 2007 recommendations of the International Commission on Radiological Protection. ICRP Publication 103. Ann ICRP. 2007;37(2–4)1–332.

33. Piccardo A, Paparo F, Piccazzo R, et al. Value of fused 18F-Choline-PET/MRI to evaluate prostate cancer relapse in patients showing biochemical recurrence after EBRT: preliminary results. Biomed Res Int. 2014;2014:103718.

34. Paparo F, Piccardo A, Bacigalupo L, et al. Value of bimodal(18)F-choline-PET/ MRI and trimodal (18)F-choline-PET/MRI/TRUS for the assessment of prostate cancer recurrence after radiation therapy and radical prostatectomy. Abdom Imaging. 2015;40:1772–87.

35. Siegel JA, Thomas SR, Stubbs JB, et al. MIRD Pamphlet No. 16: techniques for quantitative radiopharmaceutical biodistribution data acquisition and analysis for use in human radiation dose estimates. J Nucl Med. 1999;40(2):4037S–61S.

36. Soret M, Bacharach SL, Buvat I. Partial-volume effect in PET tumor imaging. J Nucl Med. 2007;48:932–45.

37. Alavi AR, Rahmim OG, Zaidi H. Partial volume correction strategies in pet. PET clinics. 2007;2(2):235–49.

38. Geworski L, Knoop BO, De Cabrejas ML, et al. Recovery correction for quantitation in emission tomography: a feasibility study. Eur J Nucl Med. 2000;27:161–9.

39. Srinivas SM, Dhurairaj T, Basu S, et al. A recovery coefficient method for partial volume correction of pet images. Ann Nucl Med. 2009;23:341–8.

40. Loevinger R, Berman M. A revised schema for calculating the absorbed dose from biologically distributed radionuclides. MIRD pamphlet no. I. New York: Society of Nuclear Medicine; 1976.

41. Snyder WS, Ford MR, Warner GG, et al. S absorbed dose per unit cumulated activity for selected radionuclides and organs. MIRD pamphlet no. 11. New York: Society of Nuclear Medicine; 1975.

42. Stabin MG, Sparks RB, Crowe E. OLINDA/EXM: the second-generation personal computer software for internal dose assessment in nuclear medicine. J Nucl Med. 2005;46:1023–7.

43. Stabin MG. Fundamentals of Nuclear Medicine Dosimetry. New York: Springer-Verlag; 2008. eBook ISBN 978–0–387-74579-4.

44. Cristy M. Active bone marrow distribution as a function of age in humans. Phys Med Biol. 1981;26:389–400.

45. Kahra D, Mondol T, Niemiec MS, et al. Human copper chaperone Atox1 translocates to the nucleus but does not bind DNA in vitro. Protein Pept Lett. 2015;22:532–8.

46. Beaino W, Guo Y, Chang AJ, et al. Roles of Atox1 and p53 in the trafficking of copper-64 to tumor cell nuclei: implications for cancer therapy. J Biol Inorg Chem. 2014;19:427–38.

47. Eiblmaier M, Meyer LA, Anderson CJ. The role of p53 in the trafficking of copper-64 to tumor cell nuclei. Cancer Biol Ther. 2008;7:63–9.

48. Sastry KS. Biological effects of the Auger emitter iodine-125: a review. Med Phys. 1992;19:1361–70. Report No. 1 of AAPM Nuclear Medicine Task Group No. 6.

49. Humm JL, Howell RW, Rao DV. Dosimetry of Auger-electron-emitting radionuclides: Report No. 3 of AAPM Nuclear Medicine Task Group No. 6. Med Phys. 1994;21(Issue 12):1901–15.

50. Makrigiorgos GM, Adelstein SJ, Kassis AI. Limitations of conventional internal dosimetry at the cellular level. J Nucl Med. 1989;30:1856–64.

51. Adelstein SJ, Kassis AI, Sastry KSR. Cellular vs. organ approaches to dose estimates. In: Proceedings of the Fourth International Radiopharmaceutical Dosimetry Symposium. Oak Ridge, 1985:477–492.

52. Kassis AI, Adelstein SJ, Haydock C, et al. Lethality of Auger electrons from the decay of bromine-77 in the DNA of mammalian cells. Radiat Res. 1982; 90:362–73.

53. Kassis AI, Adelstein SJ, Haydock C, et al. Thallium-20l: an experimental and a theoretical radiobiological approach to dosimetry. J Nud Med. 1983;24: 1164–75.

54. Kassis AI, Sastry KSR, Adelstein SJ. Intracellular distribution and radiotoxicity of chromium-51 in mammalian cells: Auger-electron dosimetry. J Nucl Med. 1985;26:59–67.

55. Kassis AI, Adelstein SJ, Haydock C, et al. Radiotoxicity of ^{75}Se and ^{35}S; theory and application to a cellular model. Radiat Res. 1980;84:407–25.

56. Chan PC, Lisco E, Lisco H, et al. The radiotoxicity of iodine-l25 in mammalian cells. II. A comparative study on cell survival and cytogenetic responses to ^{125}IUdR, ^{131}IUdR, ^{3}HTdR. Radial Res. 1976;67:332–43.

57. Hofer KG, Hughes WL. Radiotoxicity of intracellular tritium, ^{125}iodine and ^{131}iodine. Radiat Res. 1971;47:94–109.

58. Burki HJ, Rotts R, Feinendegen LE, et al. Inactivation of mammalian cells after disintegrations of ^{3}H or ^{125}I in cell DNA at −196°C. Int J Radial Biol. 1973;24:363–75.

59. Bradley EW, Chan PC, Adelstein SJ. The radiotoxicity of iodine-l25 in mammalian cells. I. Effects on the survival curve of radioiodine incorporated into DNA. Radiat Res. 1975;64:555–63.

60. Hofer KG, Harris CR, Smith JM. Radiotoxicity of intracellular ^{67}Ga ^{125}I and ^{3}H. Nuclear versus cytoplasmic radiation effects in murine L121O leukemia. Int J Radiation Biol. 1975;28:225–41.

61. Roger WH. Auger processes in the 21st century. Int J Radiat Biol. 2008; 84(12):959–75.

62. ICRP, 1988. Radiation Dose to Patients from Radiopharmaceuticals. ICRP Publication 53. Ann. ICRP 18 (1–4).

63. Avila-Rodriguez MA, Rios C, Carrasco-Hernandez J, et al. Biodistribution and radiation dosimetry of [64Cu]copper dichloride: first-in-human study in healthy volunteers. EJNMMI Res. 2017;7(1):98.